

Non-isothermal Flow through a Curved Rectangular Duct for Large Grashof Number

*Rabindra Nath Mondal**, *Md. Sharif Uddin* and *Ariful Islam*

Mathematics Discipline; Science, Engineering and Technology School,
Khulna University, Khulna-9208, Bangladesh.

*Corresponding author: rnmondal71@yahoo.com

Received February 25, 2008; accepted May 18, 2008

ABSTRACT

Non-isothermal flow through a curved rectangular duct of differentially heated vertical sidewalls is investigated numerically by using the spectral method, and covering a wide range of the Dean number, Dn , $0 < Dn \leq 1000$, and the Grashof number, Gr , $1000 \leq Gr \leq 2000$. After a comprehensive survey over the parametric ranges, five branches of asymmetric steady solutions are obtained with two- and multi-vortex solutions by using the Newton-Raphson iteration method. Linear stability of the steady solutions is then investigated. When there is no stable steady solution, time evolution calculations are performed, and it is found that for any Gr in the range, the steady flow turns into chaos through various flow instabilities, if Dn is increased.

Keywords: *Curved duct, secondary flow, steady solutions, linear stability, time-evolution.*

1. Introduction

The study of flows through a curved duct is of fundamental importance because of its numerous applications in fluids engineering, such as in heat exchangers, ventilators, gas turbines, aircraft intakes and centrifugal pumps. The flow through a curved duct shows physically interesting features under the action of the centrifugal force caused by the curvature of the duct. The earliest studies on curved pipes to predict the onset of secondary flows and its characteristics were began by Dean [2], who first formulated the problem in mathematical terms under the fully developed flow condition. Since then, there have been a lot of theoretical and experimental works concerning this flow.

One of the interesting phenomena of the flow through a curved duct is the bifurcation of the flow because generally there exist many steady solutions due to channel curvature. Studies of the flow through a curved duct have been made, experimentally or numerically, for various shapes of the cross section. However, an extensive treatment of the bifurcation structure of the flow through a curved duct of rectangular cross section was presented by Winters [9], Daskopoulos and Lenhoff [1] and Mondal [5].

Time dependent behavior of the fully developed curved duct flows was initiated by Yanase et al. [10] for a rectangular cross section in connection with the

bifurcation diagram of steady solutions. In the study they investigated unsteady solutions for the case where dual solutions exist. Wang and Yang [8] performed numerical as well as experimental investigations of periodic oscillations for the fully developed flow in a curved square duct. They showed that a temporal oscillation takes place between symmetric/asymmetric 2-cell and 4-cell flows when there are no stable steady solutions. Very recently, Mondal et al. [7] performed numerical prediction of the unsteady solutions by time-evolution calculations and showed that the steady flow turns into chaos through periodic or multi-periodic flows if the Dean number is increased. They also showed that the periodic or the chaotic state is retarded with an increase of curvature.

A remarkable characteristic of the flow through a curved duct is to enhance heat transfer from the heated wall to the fluid. Recently, Yanase et al. [11] performed numerical prediction of isothermal and non-isothermal flows through a curved rectangular duct of aspect ratio 2, where they found multiple branches of steady solutions and discussed transitional behavior of the unsteady solutions. In the succeeding paper, Yanase et al. [12] extended their work for moderate Grashof numbers and studied the effects of secondary flows on convective heat transfer. Very recently, Mondal et al. [6] performed numerical investigation of non-isothermal flow through a curved square duct for the Grashof number $Gr = 100$, where they showed that secondary flow enhances heat transfer from the heated wall to the fluid. From the scientific as well as engineering point of view, it is quite interesting to study curved duct flows with differentially heated vertical sidewalls for the large Grashof number, because this type of flow is often encountered in engineering applications.

In the present paper, a numerical study is presented for the fully developed two-dimensional flow of viscous incompressible fluid through a curved rectangular duct with differentially heated vertical sidewalls. Flow characteristics are studied over a wide range of the Dean number and the Grashof number by finding the steady solutions, investigating their linear stability and analyzing nonlinear behavior of the unsteady solutions by time evolution calculations.

2. Governing Equations

Consider an incompressible viscous fluid streaming through a curved duct of constant curvature. The cross section of the duct is a rectangle with width $2d$ and height $2h$. It is assumed that the outer wall of the duct is heated while the inner one is cooled. The temperature of the outer wall is $T_0 + \Delta T$ and that of the inner wall is $T_0 - \Delta T$, where $\Delta T > 0$. The x , y and z axes are taken to be in the horizontal, vertical, and axial directions, respectively. It is assumed that the flow is uniform in the z -direction and that it is driven by a constant pressure gradient G along center-line of the duct, i.e., the main flow in the z -direction as shown in Fig. 1.

The variables are non-dimensionalized by using of the representative length d , the representative velocity $U_0 = \nu/d$, where ν is the kinematic viscosity of the fluid. We introduce the non-dimensional variables defined as

$$u = \frac{u'}{U_0}, \quad v = \frac{v'}{U_0}, \quad w = \frac{\sqrt{2\delta}}{U_0} w', \quad x = \frac{x'}{d}, \quad y = \frac{y'}{d}, \quad z = \frac{z'}{d}$$

$$T = \frac{T'}{\Delta T}, \quad t = \frac{U_0}{d} t', \quad \delta = \frac{d}{L}, \quad P = \frac{P'}{\rho U_0^2}, \quad G = -\frac{\partial P'}{\partial z'} \frac{d}{\rho U_0^2}.$$

where u , v and w are the non-dimensional velocity components in the x , y and z directions, respectively; t is the non-dimensional time, P the non-dimensional pressure, and δ is the non-dimensional curvature. Temperature is non-dimensionalized by ΔT . Henceforth all the variables are non-dimensionalized if not specified.

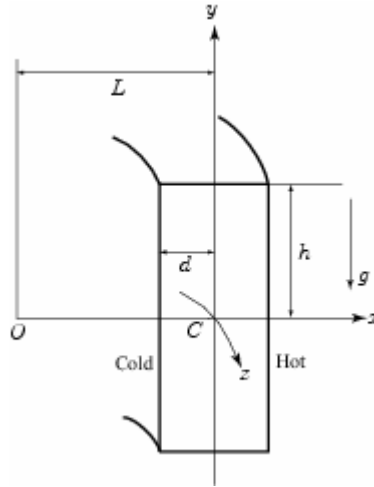


Fig. 1. Coordinate system of the curved rectangular duct

Since the flow field is uniform in the z -direction, the sectional stream function ψ is introduced as follows:

$$u = \frac{1}{1 + \delta x} \frac{\partial \psi}{\partial y}, \quad v = -\frac{1}{1 + \delta x} \frac{\partial \psi}{\partial x} \quad (1)$$

A new coordinate variable y' is introduced in the y -direction as $y = ly'$, where $l = \frac{h}{d}$ is the aspect ratio of the duct cross section. From now on, y denotes y' for the sake of simplicity. Then the basic equations for w , ψ and T are derived from the Navier-Stokes equations and the energy equation with the *Boussinesq approximation* as,

$$(1 + \delta x) \frac{\partial w}{\partial t} + \frac{1}{l} \frac{\partial (w, \psi)}{\partial (x, y)} - D_n + \frac{\delta^2 w}{1 + \delta x} = (1 + \delta x) \Delta_2 w - \frac{\delta}{l(1 + \delta x)} \frac{\partial \psi}{\partial y} w + \delta \frac{\partial w}{\partial x}, \quad (2)$$

$$\begin{aligned} & \left(\Delta_2 - \frac{\delta}{1+\delta x} \frac{\partial}{\partial x} \right) \frac{\partial \psi}{\partial t} = - \frac{1}{l(1+\delta x)} \frac{\partial(\Delta_2 \psi, \psi)}{\partial(x, y)} + \frac{\delta}{l(1+\delta x)^2} \\ & \times \left[\frac{\partial \psi}{\partial y} \left(2\Delta_2 \psi - \frac{3\delta}{1+\delta x} \frac{\partial \psi}{\partial x} + \frac{\partial^2 \psi}{\partial x^2} \right) - \frac{\partial \psi}{\partial x} \frac{\partial^2 \psi}{\partial x \partial y} \right] + \frac{\delta}{(1+\delta x)^2} \\ & \times \left[3\delta \frac{\partial^2 \psi}{\partial x^2} - \frac{3\delta^2}{1+\delta x} \frac{\partial \psi}{\partial x} \right] - \frac{2\delta}{(1+\delta x)} \frac{\partial}{\partial x} \Delta_2 \psi + \frac{1}{l} w \frac{\partial w}{\partial y} \\ & + \Delta_2^2 \psi - Gr(1+\delta x) \frac{\partial T}{\partial x}, \end{aligned} \quad (3)$$

$$\frac{\partial T}{\partial t} + \frac{1}{l(1+\delta x)} \frac{\partial(T, \psi)}{\partial(x, y)} = \frac{1}{Pr} \left(\Delta_2 T + \frac{\delta}{1+\delta x} \frac{\partial T}{\partial x} \right), \quad (4)$$

where

$$\Delta_2 \equiv \frac{\partial^2}{\partial x^2} + \frac{1}{l^2} \frac{\partial^2}{\partial y^2}, \quad \frac{\partial(f, g)}{\partial(x, y)} \equiv \frac{\partial f}{\partial x} \frac{\partial g}{\partial y} - \frac{\partial f}{\partial y} \frac{\partial g}{\partial x}. \quad (5)$$

The Dean number, Dn , the Grashof number, Gr , and the Prandtl number Pr , which appear in Eqs. (2) - (4), are defined as

$$Dn = \frac{Gd^3}{\mu\nu} \sqrt{\frac{2d}{L}}, \quad Gr = \frac{\gamma g \Delta T d^3}{\nu^2}, \quad Pr = \frac{\nu}{\kappa}. \quad (6)$$

where μ , γ , κ and g are the viscosity, the coefficient of thermal expansion, the coefficient of thermal diffusivity and the gravitational acceleration, respectively.

The rigid boundary conditions for w and ψ are

$$w(\pm 1, y) = w(x, \pm 1) = \psi(\pm 1, y) = \psi(x, \pm 1) = \frac{\partial \psi}{\partial x}(\pm 1, y) = \frac{\partial \psi}{\partial y}(x, \pm 1) = 0, \quad (7)$$

and the conducting boundary conditions for T are assumed as

$$T(1, y) = 1, \quad T(-1, y) = -1, \quad T(x, \pm 1) = x. \quad (8)$$

In the present study, Dn and Gr are varied, while δ , Pr and l are fixed as $\delta = 0.1$, $Pr = 7.0$ (water) and $l = 2$.

3. Method of Numerical Calculation

The method adopted in the present numerical calculation is the spectral method. By this method the variables are expanded in the series of functions consisting of Chebyshev polynomials. Details of this method are discussed by Mondal [5]. By this method, the expansion functions $\Phi_n(x)$ and $\Psi_n(x)$ are expressed as

$$\Phi_n(x) = (1-x^2) C_n(x), \quad \Psi_n(x) = (1-x^2)^2 C_n(x), \quad (9)$$

where $C_n(x) = \cos(n \cos^{-1}(x))$ is the n -th order Chebyshev polynomial. $w(x, y, z)$, $\psi(x, y, t)$ and $T(x, y, t)$ are expanded in terms of the functions $\Phi_n(x)$ and $\Psi_n(x)$ as

$$\left. \begin{aligned} w(x, y, z) &= \sum_{m=0}^M \sum_{n=0}^N w_{mn}(t) \Phi_m(x) \Phi_n(y), \\ \psi(x, y, t) &= \sum_{m=0}^M \sum_{n=0}^N \psi_{mn}(t) \Psi_m(x) \Psi_n(y), \\ T(x, y, t) &= \sum_{m=0}^M \sum_{n=0}^N T_{mn}(t) \Phi_m(x) \Phi_n(y) + x, \end{aligned} \right\} \quad (10)$$

where M and N are the truncation numbers in the x - and y -directions, respectively. The collocation points are taken to be

$$x_i = \cos \left[\pi \left(1 - \frac{i}{M+2} \right) \right], \quad y_j = \cos \left[\pi \left(1 - \frac{j}{N+2} \right) \right] \quad (11)$$

where $i = 1, \dots, M+1$ and $j = 1, \dots, N+1$. In the present numerical calculations, $M = 20$ and $N = 40$ have been used for sufficient accuracy of the solutions. To obtain the steady solutions, we use Newton-Raphson iteration method and to calculate the unsteady solutions, we use the Crank-Nicolson and Adams-Bashforth methods together with the function expansion (10) and the collocation method.

4. Resistance Coefficient

In the present study, the resistance coefficient λ is used as the representative quantity of the flow state. It is also called the *hydraulic resistance coefficient*, and is generally used in fluid engineering, defined as

$$\frac{P_1^* - P_2^*}{\Delta z^*} = \frac{\lambda}{dh^*} \frac{1}{2} \rho \langle w^* \rangle^2, \quad (12)$$

where quantities with an asterisk denote the dimensional ones, $\langle \rangle$ stands for the mean over the cross section of the rectangular duct, ρ the density, and $d_h^* = 4(2d \times 4d)/(4d \times 8d)$ is the hydraulic diameter. The mean axial velocity $\langle w^* \rangle$ is calculated by

$$\langle w^* \rangle = \frac{\nu}{4\sqrt{2}\delta d} \int_{-1}^1 dx \int_{-1}^1 w(x, y, t) dy \quad (13)$$

Since $(P_1^* - P_2^*)/\Delta z^* = G$, λ is related to the mean non-dimensional axial velocity $\langle w \rangle$ as

$$\lambda = \frac{8l\sqrt{2}\delta Dn}{(1+l)\langle w \rangle^2}, \quad (14)$$

where $\langle w \rangle = \sqrt{2}\delta d \langle w^* \rangle / \nu$. In this paper, λ is used to discriminate the steady solution branches and to pursue the time evolution of the unsteady solutions.

5. Results and Discussion

We obtain steady solutions, investigate their linear stability and perform nonlinear behavior of the unsteady solutions by time-evolution calculations. Though the present study covers a wide range of Gr ($1000 < Gr \leq 2000$), in the present paper, however, a single the case of the Grashof numbers, $Gr = 2000$, is discussed in detail, and a schematic diagram for the distribution of the steady and unsteady solutions, obtained by the time evolution calculations, is presented in the Dean number vs. Grashof number plane for $0 \leq Dn \leq 1000$ and $1000 \leq Gr \leq 2000$.

5.1. Steady solutions

With the present numerical calculations, five branches of asymmetric steady solutions are obtained by the path continuation technique with various initial guesses as discussed by Mondal [5]. Figure 2(a) shows bifurcation diagram of the steady solutions for $Gr = 2000$ and $100 \leq Dn \leq 1000$. The steady solution branches are named the *first steady solution branch* (first branch, thick solid line), the *second steady solution branch* (second branch, thin solid line), the *third steady solution branch* (third branch, dash dotdot line), the *fourth steady solution branch* (fourth branch, dashed line) and the *fifth steady solution branch* (fifth branch, dash dotted line), respectively. In order to see the intricate branch structure and to distinguish the steady solution branches from each other, an enlargement of Fig. 2(a) is shown in Fig. 2(b) at larger Dn , where it is observed that the steady solution branches are independent and there exists no bifurcating relationship among the branches in the parameter range investigated in this paper. It is found that the first branch is composed of one- and two-vortex solutions. The second branch consists of two- and four- vortex solutions. The third branch is characterized by two- and four-vortex solutions, but different from the second branch in the form of vortices generated near the outer wall. The fourth branch contains two-, four- and six-vortex solutions and the fifth branch two-, four-, six- and eight-vortex solutions.

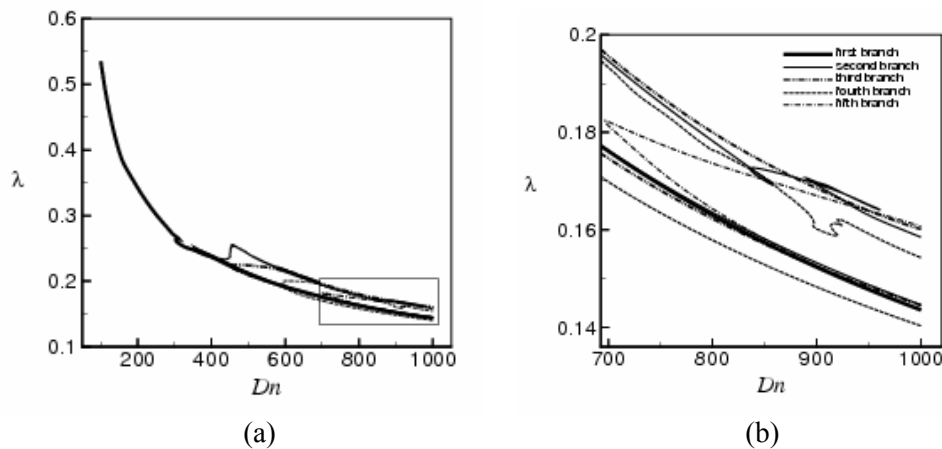


Fig. 2. (a) Steady solution branches for $Gr = 2000$ and $100 \leq Dn \leq 1000$ (thick solid line: first branch, thin solid line: second branch, dash dotdot line: third branch, dashed line: fourth branch, dash dotted line: fifth branch). (b) Enlargement of (a) at larger Dean numbers ($695 \leq Dn \leq 1000$).

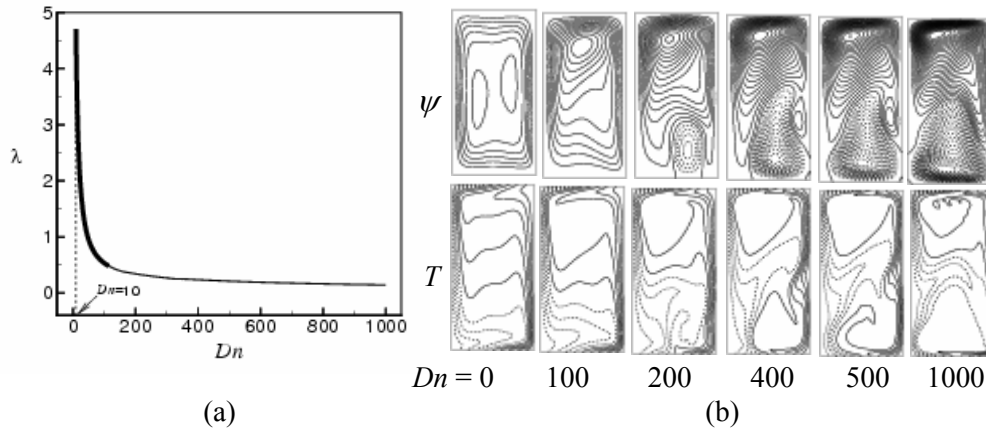


Fig. 3. (a) First steady solution branch ($10 \leq Dn \leq 1000$) with the region of linear stability (bold line), (b) contours of secondary flow (top) and temperature profile (bottom) for the first steady solution branch for $Gr = 2000$ and $0 < Dn \leq 1000$.

The first steady solution branch is exclusively depicted in Fig. 3(a) for $10 \leq Dn \leq 1000$. Among five branches of steady solutions, this is the only branch exists throughout the whole range of the Dean numbers investigated in this paper. To observe the change of the flow patterns and temperature distributions, contours of typical secondary flow and temperature profile at several Dn 's are shown in Fig. 3(b), where the contours of ψ and T are drawn with the increments $\Delta\psi = 0.6$ and $\Delta T = 0.2$, respectively. The same increments of ψ and T are used for all the figures in this paper, if not specified. As seen in Fig. 3(b), the first steady solution branch contains one- and two-vortex solutions which are asymmetric with respect to the horizontal centre plane $y = 0$. Heating the outer wall causes deformation of the secondary flow and yields asymmetry of the flow.

5.2 Linear stability of the steady solutions

In the present study, linear stability of the steady solutions is investigated against only two-dimensional perturbations. To do this, the eigenvalue problem is solved which is constructed by the application of the function expansion method together with the collocation method to the perturbation equations obtained from Eqs. (2), (3) and (4). It is assumed that the time dependence of the perturbation is $e^{i\sigma}$, where $\sigma = \sigma_r + \sigma_i$ is the eigenvalue with σ_r the real part, σ_i the imaginary part and $i = \sqrt{-1}$. If all the real parts of the eigenvalue σ are negative, the steady solution is linearly stable, but if there exists at least one positive real part of the eigenvalue, it is linearly unstable. In the unstable region, the perturbation grows monotonically for $\sigma_i = 0$ and oscillatory for $\sigma_i \neq 0$.

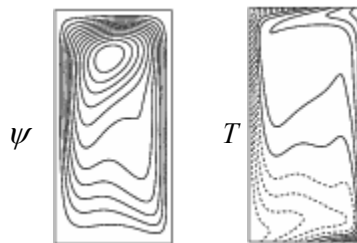
Table 1. Linear stability of the first steady solution branch for $Gr = 2000$.

Dn	λ	σ_r	σ_i
0	0.000000	-9.6536×10^{-1}	0
50	0.962074	-1.0095×10^{-1}	0
100	0.535108	-1.0010×10^{-1}	0
115	0.481988	-3.2498×10^{-2}	$\pm 1.087 \times 10$
116	0.478959	1.5081×10^{-1}	$\pm 1.096 \times 10$
300	0.269664	8.2333	$\pm 1.060 \times 10$
500	0.210999	2.3734×10	± 3.844
1000	0.143630	5.8754×10	$\pm 4.508 \times 10$

On the basis of the above-mentioned criterion, linear stability of the steady solutions is studied. It is found that among five branches of steady solutions; only the first branch is linearly stable while the other branches are linearly unstable. Eigenvalues of the first steady solution branch are shown in Table 1, where the eigenvalues with the maximum real part of σ are presented. Those for the linearly stable solutions are printed in bold letters. As seen in Table 1, the stability region exists for $0 \leq Dn \leq 115$. Linearly stable steady solution region is shown with thick solid line in Fig. 3(a). It is found that the *Hopf bifurcation* occurs at $Dn \approx 115$.

5.3 Time evolution

In order to study the nonlinear behavior of the unsteady solutions, time evolution calculations of the velocity and temperature fields are performed for $Gr = 2000$ at $Dn = 100, 200, 400, 450, 500, 600$ and 1000 . It is found that the flow approaches a steady state solution for $Dn = 100$, no matter what the initial condition we use. A single contour of the secondary flow and temperature profile for $Dn = 100$ at time $t = 8$ is shown in Fig. 4, where it is observed that the flow is a single-vortex solution which closely agrees with the steady solution on the first branch at $Dn = 100$, which is linearly stable.

**Fig. 4.** Contours of secondary flow (left) and temperature profile (right) for $Gr = 2000$ at time $t = 8$.

Time evolution of λ together with the value of λ for the first steady solution branch, indicated by straight line, is shown in Fig. 5(a) for $Dn = 200$. Figure 5(a) shows that the flow is periodic, which takes place above the first steady solution branch. To observe the periodic change of the flow pattern, contours of typical secondary flow and temperature profile are shown in Fig. 5(b) for $Dn = 200$ which

shows that the periodic oscillation at $Dn = 200$ is a two-vortex solution. Time evolution of λ for $Dn = 400$ is shown in Fig. 6(a). This figure shows that the flow oscillates irregularly which suggests that the flow is chaotic. As seen in Fig. 6(a), the chaotic solution at $Dn = 400$ fluctuates around $\lambda = 0.24$ above the first steady solution branch and this branch seems to be an envelope of this chaotic solution. Contours of secondary flow and temperature distribution for $Dn = 400$ are shown in Fig. 6(b) for $15 \leq t \leq 17.5$. Time evolution of λ is then performed for $Dn = 450$ as shown in Fig. 7(a). It is found that the flow again turns into time periodic. To explore the relationship between the periodic solution and the steady states, steady values of λ on the steady solution branches at $Dn = 450$ are also shown with straight lines, and it is seen that the periodic solution at $Dn = 450$ drifts in the region between the upper and lower parts of the second steady solution branch. Contours of typical secondary flow and temperature profile are shown in Fig. 7(b) for $Dn = 450$.

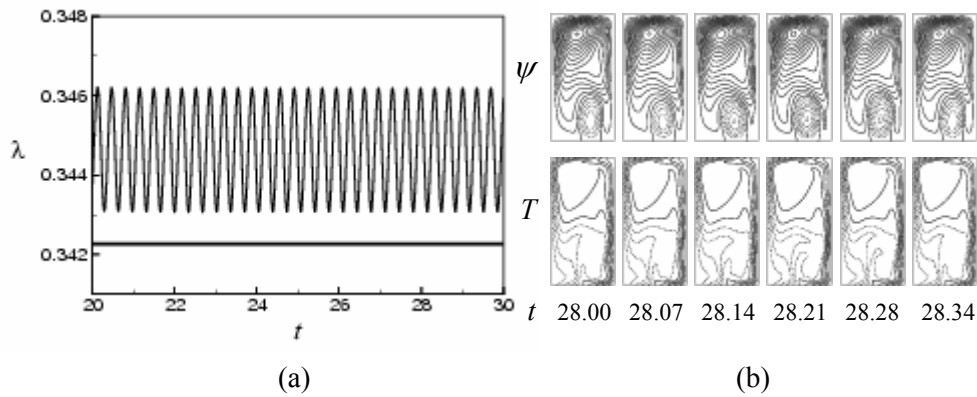


Fig. 5. The results for $Gr = 2000$ and $Dn = 200$. (a) Time evolution of λ and the value of λ for the first steady solution for $20 \leq t \leq 30$, (b) contours of secondary flow (top) and temperature profile (bottom) for one period of oscillation at $28.00 \leq t \leq 28.34$.

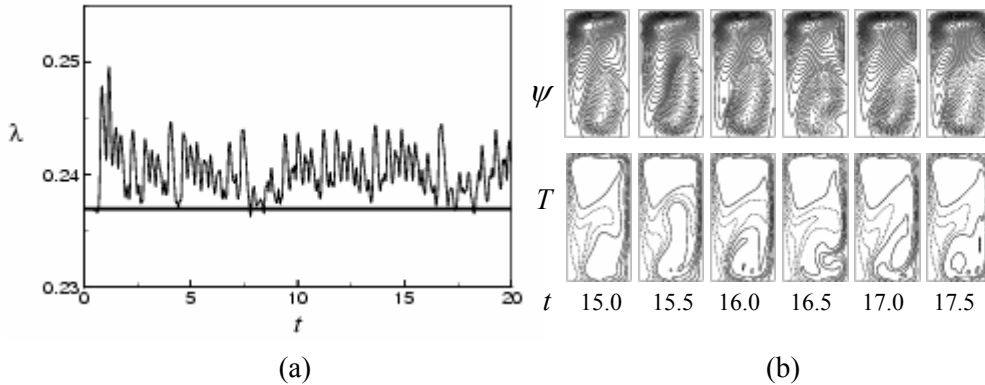


Fig. 6. The results for $Gr = 2000$ and $Dn = 400$. (a) Time evolution of λ and the value of λ for the first steady solution for $0 \leq t \leq 20$, (b) contours of secondary flow (top) and temperature profile (bottom) for one period of oscillation at $15.0 \leq t \leq 17.5$.

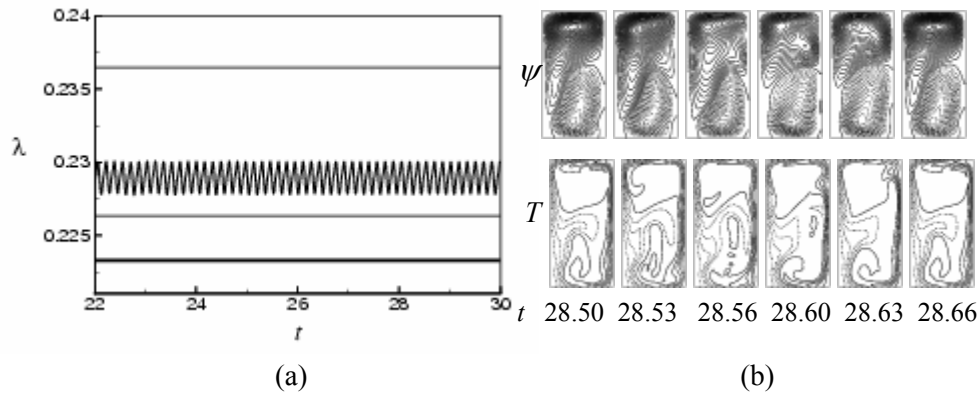


Fig. 7. The results for $Gr = 2000$ and $Dn = 450$. (a) Time evolution of λ and the value of λ for the first steady solution for $22 \leq t \leq 30$, (b) contours of secondary flow (top) and temperature profile (bottom) for one period of oscillation at $28.50 \leq t \leq 28.66$.

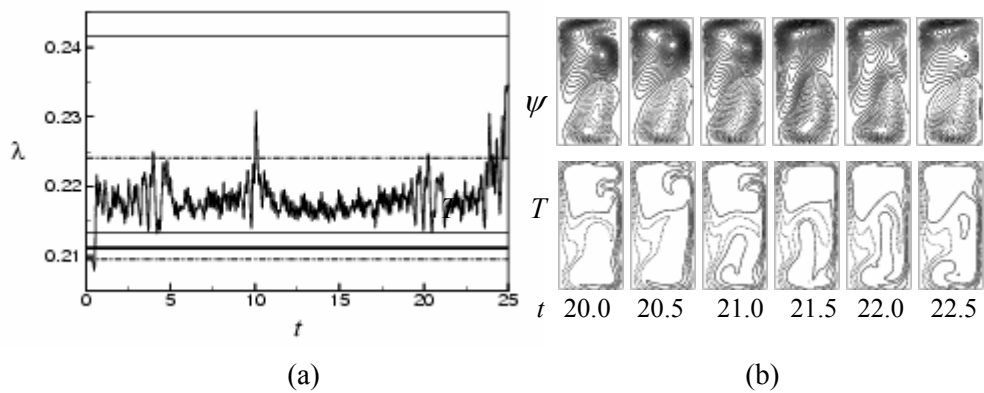


Fig. 8. The results for $Gr = 2000$ and $Dn = 500$. (a) Time evolution of λ and the value of λ for the first steady solution for $0 \leq t \leq 25$, (b) contours of secondary flow (top) and temperature profile (bottom) for one period of oscillation at $20.0 \leq t \leq 22.5$.

Next, time evolution of λ for $Dn = 500$ is conducted as shown in Fig. 8(a). Figure 8(a) shows that the flow again turns into chaotic. To comprehend the relationship between the chaotic solution and the steady states, steady values of λ on the steady solution branches at $Dn = 500$ are also shown which are indicated by straight lines using the same kind of lines as were used in the bifurcation diagram in Fig. 2. It is found that the chaotic solution at $Dn = 500$ oscillates in the region between the second and third steady solution branch. To observe the change of the flow characteristics, as time proceeds, contours of typical secondary flow and temperature profile for $Dn = 500$ are shown in Fig. 8(b). Time evolution of λ is then performed for $Dn = 1000$ as shown in Fig. 9(a). In this figure, the steady values of λ for the steady solution branches at $Dn = 1000$ are also shown. Figure 9(a) shows

that the unsteady flow at $Dn = 1000$ is also chaotic, which moves around $\lambda = 0.1655$ above all the steady solution branches and the steady solution branch having the maximum λ ($\lambda = 0.1607$, upper part of the fifth steady solution branch) looks like an envelope of this chaotic solution. The chaotic solution for $Dn = 500$ is called a ‘weak chaos’ but that for $Dn = 1000$ a ‘strong chaos’ (Mondal *et al.* [7]), because the chaotic solution at $Dn = 500$ is still trapped by the steady solution branches but that for $Dn = 1000$ tends to get away from them. Thus it is suggested that occurrence of the chaotic state is related with destabilization of the steady solutions, which reminds us the case of Lorenz chaos [3]. In this regard, it is worth mentioning that irregular oscillation of isothermal flows through a curved rectangular duct has been observed experimentally by Ligrani and Niver [4] for the large aspect ratio. To observe the change of the flow patterns, contours of typical secondary flow and temperature profile are shown in Fig. 9(b) for $Dn = 1000$ at $6.0 \leq t \leq 8.0$, where the increments $\Delta\psi = 1.2$ and $\Delta T = 0.4$ have been used for $Dn = 1000$.

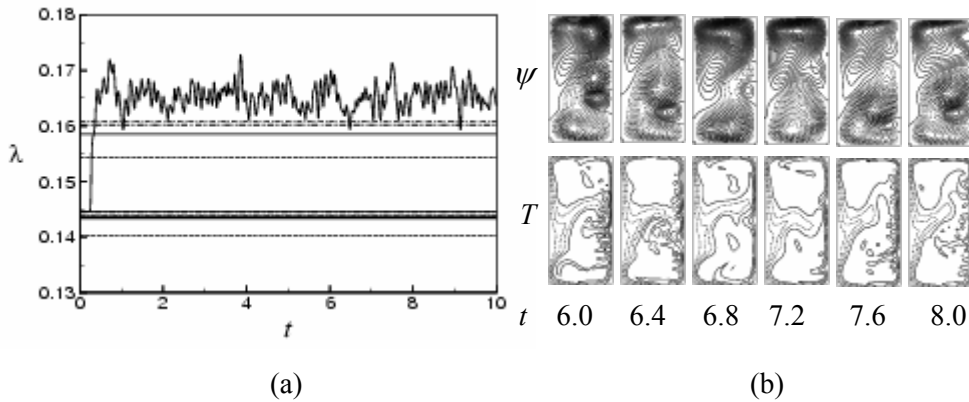


Fig. 9. The results for $Gr = 2000$ and $Dn = 1000$. (a) Time evolution of λ and the value of λ for the first steady solution for $0 \leq t \leq 10$, (b) contours of secondary flow (top) and temperature profile (bottom) for one period of oscillation at $6.0 \leq t \leq 8.0$.

5.4 Phase diagram in the $Dn-Gr$ plane

Finally, the distribution of the time-dependent solutions, obtained by the time evolution calculations of the flow, is shown in Fig. 10 in the Dean number vs. Grashof number plane ($Dn - Gr$ plane) for $0 \leq Dn \leq 1000$ and $1000 \leq Gr \leq 2000$. In this picture, the circles indicate the steady-state solution, the crosses periodic solutions and the triangles chaotic solution. As seen in Fig. 10, the steady flow turns into chaos through various flow instabilities, if Dn is increased keeping Gr fixed. At some Gr ($1000 \leq Gr \leq 2000$), however, sometimes there exist three or two exclusive regions of Dn where the solution is time periodic, and at $Gr = 2000$ the flow undergoes in the scenario *steady* \rightarrow *periodic* \rightarrow *chaotic* \rightarrow *periodic* \rightarrow *chaotic*, if Dn is increased. It is also found that, if Gr is increased further

($Gr > 2000$), the regions of periodic solutions shrink and consequently the regions of chaotic solutions expand.

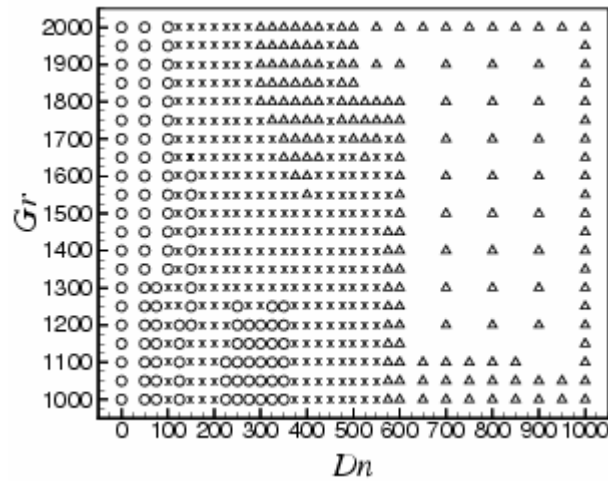


Fig. 10. Distribution of the time-dependent solutions in the Dean number vs. Grashof number ($Dn-Gr$) plane for $0 \leq Dn \leq 1000$ and $1000 \leq Gr \leq 2000$ (O : steady-state solution, x : periodic solution, Δ : chaotic solution).

6. Conclusions

In this paper, a detailed numerical study of the non-isothermal flow through a curved rectangular duct of aspect ratio 2 has been presented by using the spectral method over a wide range of the Dean number $0 < Dn \leq 1000$ and the Grashof number $1000 \leq Gr \leq 2000$ for the curvature $\delta = 0.1$.

After a comprehensive survey over range of the parameters, five branches of asymmetric steady solutions are obtained. Linear stability analysis shows that among five branches of steady solutions, only the first branch is linearly stable, while the other branches are linearly unstable. It is found that the *Hopf bifurcation* occurs at the Dean numbers on the boundary where stability disappears. Time evolutions of the flow show that, the steady flow turns into chaos through various flow instabilities, if Dn is increased keeping Gr fixed. It is found that, there exist three or two exclusive regions of Dn where the solution is time periodic. If Gr is increased further ($Gr > 2000$), the region of chaotic solution expands and consequently the regions of periodic solutions merge into a single region of periodic solution.

REFERENCES

1. Daskopoulos, P. and Lenhoff, A. M., *Flow in curved ducts: bifurcation structure for stationary ducts*, J. Fluid Mech., **203**(1989), 125--148.
2. Dean, W. R., *Note on the motion of fluid in a curved pipe*, Philos. Mag., **4**(1927), 208--223.

3. Lorenz, E. N., *Deterministic non-periodic flow*, J. Atms. Sci., **20**(1963), 130-141.
4. Ligrani, P. M. and Niver, R. D., *Flow visualization of Dean vortices in a curved hannel with 40 to 1 aspect ratio*, Phys. Fluids, **31**(1988), 3605--3617.
5. Mondal, R. N., *Isothermal and non-isothermal flows through curved ducts with square and rectangular cross sections*, Ph.D. Thesis, Department of Mechanical Engineering, Okayama University, Japan, (2006).
6. Mondal, R. N., Kaga, Y., Hyakutake, T. and Yanase, S., *Effects of curvature and convective heat transfer in curved square duct flows*, Trans. ASME, Journal of Fluids engineering, **128**(9)(2006), 3264--3275.
7. Mondal, R. N., Kaga, Y., Hyakutake, T. and Yanase, S., *Bifurcation diagram for two-dimensional steady flow and unsteady solutions in a curved square duct*, Fluid Dyn. Res., **39**(2007), 413--446.
8. Wang, L. and Yang, T., *Periodic oscillation in curved duct flows*, Physica D, **200**(2005), 296--302.
9. Winters, K. H., *A bifurcation study of laminar flow in a curved tube of rectangular cross-section*, J. Fluid Mech., **180**(1987), 343--369.
10. Yanase, S. and Nishiyama, K., *On the bifurcation of laminar flows through a curved rectangular tube*, J. Phys. Soc. Japan, **57**(1988), 3790--3795.
11. Yanase, S., Mondal, R. N., Kaga, Y. and Yamamoto, K., *Transition from steady to chaotic states of isothermal and non-isothermal flows through a curved rectangular duct*, J. Phys. Soc. Japan, **74**(2005a), 345--358.
12. Yanase, S., Mondal, R. N. and Kaga, Y., *Numerical study of non-isothermal flow with convective heat transfer in a curved rectangular duct*, Int. J. Thermal Sci., **44**(2005b), 1047--1060